Title

Uranium isotope fractionation by abiotic reductive precipitation

Journal

Proceedings of the National Academy of Sciences of the United States of America, 115(35)

ISSN

0027-8424

Authors

Brown, Shaun T

Basu, Anirban

Ding, Xin

et al.

Publication Date

2018-08-28

DOI

10.1073/pnas.1805234115

Peer reviewed

Uranium isotope fractionation by abiotic reductive precipitation

Shaun T. Brown, Anirban Basu, Xin Ding, John N. Christensen, and Donald J. DePaolo

Significance

We use an experimental approach to demonstrate that $^{238}U/^{235}U$ is fractionated by abiotic reduction onto the surface of abiotic synthetic iron monosulfide, contradicting the findings of earlier studies. We further demonstrate that for abiotic reduction reactions the aqueous U speciation and removal rate control the extent of isotopic fractionation. U isotopic fractionation is observed when the primary aqueous species are $Ca–UO_2–CO_3$, suggesting that aqueous U speciation affects the relative forward and backward reaction rates and by extrapolation the relative roles of nuclear field shift effect and mass dependent kinetic fractionation.

Abstract

Significant uranium (U) isotope fractionation has been observed during abiotic reduction of aqueous U, counter to the expectation that uranium isotopes are only fractionated by bioassociated enzymatic reduction. In our experiments, aqueous U is removed from solution by reductive precipitation onto the surfaces of synthetic iron monosulfide. The magnitude of uranium isotopic fractionation increases with decreasing aqueous U removal rate and with increasing amounts of neutrally charged aqueous $Ca–U–CO_3$ species. Our discovery means that abiotic U isotope fractionation likely occurs in any reducing environment with aqueous Ca ≥ 1 mM, and that the magnitude of isotopic fractionation changes in response to changes in aqueous major ion concentrations that affect U speciation. Our results have implications for the study of anoxia in the ancient oceans and other environments.

Keywords: Uranium, abiotic fractionation, isotopes, isotope fractionation

Uranium isotope fractionation in the environment was historically assumed to be negligible; however, variations in $^{238}U/^{235}U$ of up to 9‰ have been documented in both experimental and natural settings (1–7). The discovery of variable $^{238}U/^{235}U$ has affected geochronology and cosmochemistry, changing the methodology for high-precision ages and proving the existence of the short-lived isotope ^{247}Cm (4, 8, 9). Variations in $^{238}U/^{235}U$ are also used for investigating biological U cycling on Earth and other planets' (10) oxidation of the Earth’s atmosphere (11), and nuclear forensics (12). Stylo et al. (10) recently concluded that microbial U reduction produced a unique U isotopic signature compared with abiotic U reduction. The finding of unique isotopic effects by microbial reduction warrants further investigation to develop the quantitative use of $^{238}U/^{235}U$ in environmental chemistry.

Although the standard mass-dependent isotope fractionation (MDF) effects for uranium isotopes are expected to be small (13, 14) and favor the lighter isotopes in the product phases, there are additional effects due to nuclear

size and shape (nuclear field shift effect; NFS) that preferentially partition the ^{238}U isotope into the lowest possible electron density configuration at the nucleus (15, 16). For example, in isotope exchange experiments where U of two oxidation states such as U(III) and U(IV) are allowed to equilibrate, the U(III) has higher $^{238}U/^{235}U$ by 2.3‰ based on experimental results and theoretical calculations (15⇓–17). This observed isotopic fractionation is presumably the sum of MDF and NFS effects. Studies aimed at replicating inorganic U isotope fractionation during reductive precipitation of U(VI) to U(IV), which most likely are not equilibrium experiments, have found either no isotope fractionation or fractionation that results in the reduced product U(IV) phase having lower $^{238}U/^{235}U$, contrary to equilibrium NFS predictions (3, 10, 18) but potentially consistent with nonequilibrium MDF. Although there is some confusion (or uncertainty) about the issue in the literature, it is likely that NFS effects are most strongly expressed in equilibrium isotopic partitioning, whereas MDF effects are likely to apply to both equilibrium and nonequilibrium (kinetically controlled) processes. Fundamental in interpreting the observed $^{238}U/^{235}U$ isotopic fractionation is understanding the chemical reactions that result in U(VI) reduction including the extent to which laboratory experiments and natural systems depart from equilibrium.

The study of chemical factors affecting U reduction in the environment is of considerable prior interest (19). With respect to abiotic reduction, the role of mineral surfaces (20), kinetic and steric effects inhibiting U reduction (21), the role for single- or two-electron transfer and accompanied U(V) disproportionation, and the effects of aqueous U speciation (22⇓–24) are thought to significantly affect the rate and efficiency of reduction. Our study focuses specifically on U speciation, because it is known to affect the efficiency of aqueous U(VI) removal from solution (25, 26).

A key issue in evaluating the consistency of the isotope exchange experiments described above is the speciation of aqueous uranium. The isotopic exchange experiments (15, 17) were conducted at low pH (<5) where the primary U(VI) and U(IV) species are both aqueous, and isotopic equilibrium between aqueous U(VI) and U(IV) is relatively fast (27). At higher pH, in the range of 6–8, and in typical aqueous solution compositions relevant to most Earth surface processes, aqueous U(VI) is primarily a mixture of multiple hydrated $U–CO_3$ and $U–M–CO_3$molecules (where M is an alkaline Earth metal such as Ca or Mg) (28, 29). For example, in the absence of dissolved calcium the primary uranyl carbonato complex is $UO_2(CO_3)_2^{2-}$, whereas in the presence of ≥1 mM calcium the primary species is the neutrally charged $Ca_2UO_2(CO_3)_3^0$ and the second most abundant species is $CaUO_2(CO_3)_3^{2-}$.

Aqueous U(VI) speciation also influences the rate of U(VI) reduction and possibly the reaction pathways (30). Previous experimental studies observed rapid U removal, consistent with sorption to the mineral surface or rapid U(VI) reduction (3, 10, 18). While these studies tested multiple reductants and variable aqueous fluid compositions (e.g., 0–100 mM HCO_3^-), one

consistent feature of the experiments was rapid removal of aqueous U(VI). What was not investigated is the effect of high-concentrations aqueous Ca^{2+}, which increase the proportion of neutral ternary calcium–uranyl–carbonato complexes that are known to be more difficult to sorb or reduce by microbial processes (25, 26, 31). Since Ca–uranyl–carbonato complexes are nearly ubiquitous in circumneutral pH waters (e.g., refs. 32 and 33), the effects of aqueous U speciation on isotopic fractionation is likely to be important in most Earth surface environments (34, 35).

Approach

To evaluate the role of aqueous U speciation on the isotopic fractionation between U(VI) and U(IV) we designed a series of abiotic U(VI) reduction experiments with synthesized mackinawite (FeS) crystals under anoxic conditions. FeS is a well-established U reductant under a variety of laboratory and environmental conditions (e.g., refs. 10 and 36). FeS was added to preequilibrated U(VI)–$NaHCO_3$–$CaCl_2$solutions (pH 7.1) that were continuously mixed for the duration of the experiments. The experimental solutions were prepared with different initial $CaCl_2$ concentrations (0–2 mM) to vary the ratio of negatively charged to neutral aqueous Ca–uranyl–carbonato complexes. All experiments had identical FeS and HCO_3^- concentrations (0.7 and 6 mM, respectively).

The postexperiment FeS particles were characterized by scanning electron microscope (SEM)–energy-dispersive spectroscopy (*SI Appendix*, Fig. S1). The Fe:S ratio is ∼1.7, consistent with other synthetic FeS (37). Uranium is observed coating the FeS particles and also elsewhere in the beaker (*SI Appendix*, Fig. S1). The U is not associated with significant amounts of Ca or CO_3 in any of the studied run products. The $^{238}U/^{235}U$ data are reported in standard stable isotope delta notation (1⇓–3) where $(^{238}U/^{235}U)_{t0}$ is the measured $^{238}U/^{235}U$ at the start of each experiment.

Results

Aqueous U speciation for each experiment was calculated using Geochemists Workbench with a modified version of the LLNL V8 R6 “combined” database, incorporating updated formation constants for ternary and carbonato uranium species (19, 28) (*SI Appendix*, Tables S1 and S2). All experiments are undersaturated in $CaCO_3$ polymorphs and the U(VI) minerals schoepite and metaschoepite. The sums of all negatively charged and neutrally charged aqueous U(VI) species were tabulated for each experiment and are reported in Table 1 as the percent of neutral uranium species ($U_{neutral}$). For the range of 0–2 mM calcium, calculated $U_{neutral}$ varies from 3 to 72% (*SI Appendix*, Fig. S1). Reduction is thermodynamically favorable in each experiment, with the Gibbs free energy (ΔG) of the half-reaction ranging from −3.7 to −17.5 kJ mol^{-1}.

Table 1. Uranium reduction experiment results

Experiment ID	Time, h	U, μmol	C/C_0	$\delta^{238}U$
EXP 1 0 mM $CaCl_2$ $U_{neutral}$ = 3%				
a0	0	8.96	1.00	0.00
a4	1	7.93	0.89	−0.06
a8	3	4.85	0.54	−0.24
a10	4	3.68	0.41	−0.37
a12	5	1.79	0.20	−0.44
EXP 2 0.5 mM $CaCl_2$, $U_{neutral}$ = 40%				
b0	0	9.44	1.00	0.00
b1	1	9.11	0.97	−0.02
b2	3	8.40	0.89	0.04
b3	6	6.75	0.71	−0.16
b4	7.5	5.46	0.58	−0.41
b5	24	0.66	0.07	−1.16
b6	27	0.15	0.02	−2.29
EXP 3 1.0 mM $CaCl_2$, $U_{neutral}$ = 57%				
a0	0	9.28	1.00	0.00
a2	3	9.16	0.99	0.17
a3	6	8.26	0.89	−0.22
a4	7.5	7.26	0.78	−0.31
a5	24	2.65	0.29	−0.91
a7	30	1.08	0.12	−1.76
a8	48	0.27	0.03	−2.28
EXP 4 2.0 mM $CaCl_2$, $U_{neutral}$ = 72%				
c0	0	9.13	1.00	0.00
c7	6	7.76	0.85	−0.25
c9	27	2.51	0.27	−1.28
c10	30	1.99	0.22	−1.45
c11	46	0.74	0.08	−2.09

All experiments have 6 mM $NaHCO_3$ and 3 mg FeS.

U(VI) concentrations decreased with time during all experiments, regardless of the solution composition (Fig. 1, Table 1, and *SI Appendix*, Fig. S2). Each experiment shows a linear correlation between ln[U] and time ($r^2 \geq 0.92$), consistent with pseudo–first-order kinetics with rate constants (k) given by the slope of the ln(U)–time relationship in each experiment (*SI Appendix*, Fig. S2). U(VI) removal half-lives [$t_{1/2} = ln\ (2)/k$] range from 2.3 h in the Ca-free experiment to 12.6 h in the 2.0 mM Ca experiment, with a correlation coefficient between $t_{1/2}$ and calcium concentration of $r^2 = 0.98$.

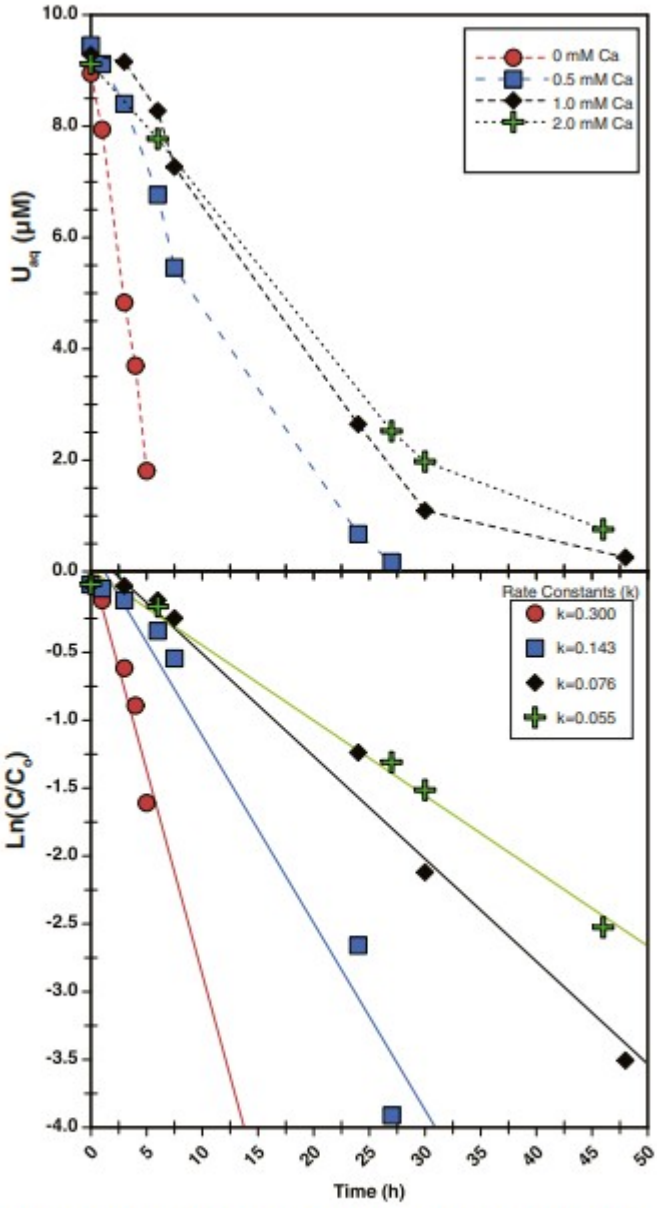

Fig. 1. (*Upper*) Dissolved U concentrations in the solution phase as a function of experiment time showing a decrease in the rate of U removal with increasing Ca concentration. (*Lower*) Linearized U concentration–time relationship used to determine the rate constant (k) in inverse hours (h^{-1}). The rate constants change by a factor of ~5 over the investigated [Ca] range of 0–2 mM.

The $\delta^{238}U$ of the aqueous U(VI) remaining in solution varies from 0‰ at the start of the experiments to as low as −2.29‰ after 98% U(VI) removal (Fig. 2 and Table 1). The U isotope fractionation factor (α) for each experiment was determined by linear least-squares regression methods (38) and varies from 1.00023 to 1.00084 (Fig. 2). These αs can also be expressed as enrichment factors (ε) where ε = 1000 ln(α). All of the αs obtained from our experiments are distinct from previously published abiotic U(VI) reduction experiments where α ≤ 1.0000 (3, 10, 18), but overlap with microbial

reduction experiments (6, 10, 39). The magnitude of U isotope fractionation is strongly correlated with the calculated $U_{neutral}$ (r^2 = 0.998, Fig. 3).

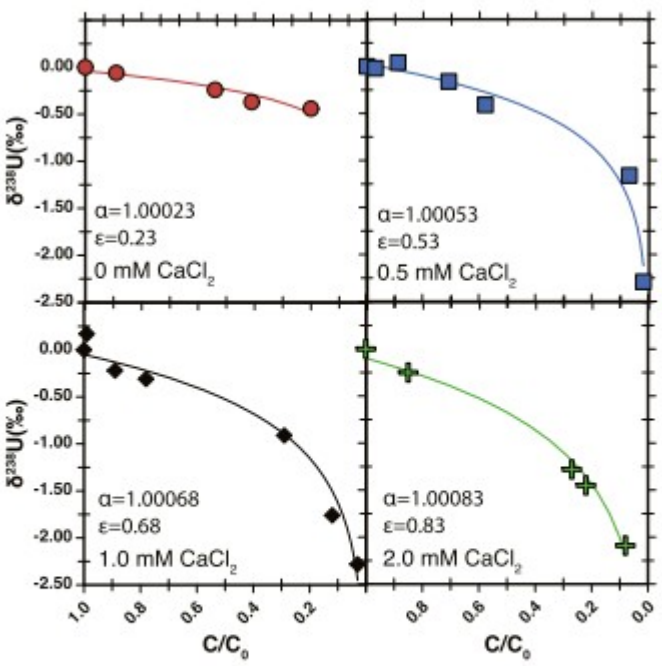

Fig. 2. $\delta^{238}U$ of dissolved uranium in the solution for each experiment as a function of remaining aqueous U fraction. Curves in each panel are the best-fit logarithmic function. Uncertainty in $\delta^{238}U$ and [U] are smaller than the symbol sizes. Fractionation factors (α) and isotope enrichment factors (ε) corresponding to the best-fit curves are given for each experiment.

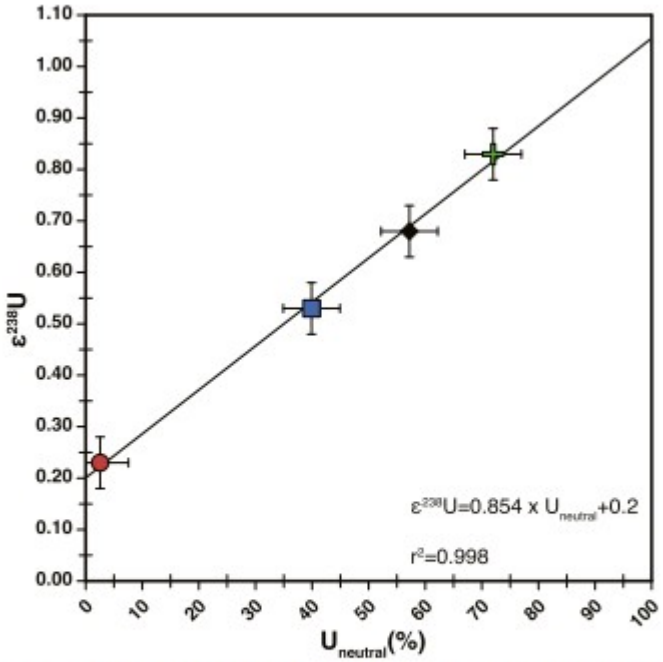

Fig. 3. Relationship between neutrally charged U species fraction in solution and U isotope fractionation factor. Uncertainties in the thermodynamic speciation models are estimated to be 5% and the calculated uncertainty of $\varepsilon^{238}U$ is ~5% (1σ) for all experiments. The observed correlation between $U_{neutral}$ and $\varepsilon^{238}U$ suggests that at high fractions of $U_{neutral}$, $\varepsilon^{238}U$ approaches the range of theoretical NFS isotope enrichment factors (~1.0–1.3‰).

Discussion

U Removal Mechanism.

The first-order rates derived from Fig. 1 are consistent with a single characteristic U removal mechanism in each experiment. If more than one removal mechanism (e.g., sorption and reduction) with distinct rates removed substantial amounts of aqueous U, a single rate constant is unlikely to fit time series. We conclude that the change in U removal rate constants in Fig. 1 is not due to changing proportions of reduction and sorption but due to a change in the rate of a single removal mechanism. This is further supported by the isotopic results where each experiment produces a single fractionation factor that fits all $\delta^{238}U$ from both early and late time (*SI Appendix*, Fig. S1). Changing proportions of sorption and reduction during the course of an experiment would result in different ε values characteristic of these mechanisms, which will make it impossible for a single ε to describe all data from an experiment. In addition, experimental studies of U sorption onto quartz and ferrihydrite confirm that varying Ca concentrations do not affect sorption rates (25), which leads us to conclude that the observed relationship between the U removal rate constant and U speciation is a change in the U reduction rate.

Earlier studies also report that in experiments with similarly synthesized FeS the final U product is U(IV) that is consistent with uraninite (10, 40⇓–42). In those studies the experiments have fluid with no dissolved Ca, and the rates of U removal are likely much faster than in our experiments since the experiments produced quantitative removal of aqueous U within several minutes. Despite these differences, the final reaction product in the presence of FeS is reduction to U(IV). Stylo et al. (10) conducted U(VI) reduction experiments with a similarly synthesized FeS where sorption initially removes U(VI) from solution rapidly, but the final solid phase is 99% UO_2 and hence must be uraninite. Furthermore, other recent studies with FeS as a reductant demonstrate by spectroscopic methods that U reduction to U(IV) and not sorption or U(VI) precipitation is the ultimate U product (40, 42).

The interpretation that sorption is insignificant in our experiments does not mean there is no sorption of aqueous U(VI), but rather that sorption must be reversible and not rate determining. The point of zero charge (PZC) condition for disordered mackinwaite is at pH 7.5, meaning that at the experiment pH of 7.1 the FeS surface charge is positive and still allows for the sorption of negatively charged U–CO_3 molecules (37). The inferred small fraction of U sorption in our experiments is different from similar studies of U(VI) reduction by FeS (e.g., ref. 10). This difference might be due to several factors including: (*i*) the lower starting U concentration in our experiments reduces the sorption rate, (*ii*) the higher HCO_3 concentration produces aqueous U–CO_3molecules less favorable for sorption, and (*iii*) the higher pH of our experiments compared with (10) results in a smaller departure from PZC, which reduces the sorption rate. For example, the proton balance on the FeS surface is at least 50% lower in our experiments compared with those of ref. 10.

U Isotope Fractionation Mechanism.

The $^{238}U/^{235}U$ isotope ratio shifts of aqueous U(VI) in our experiments require that U(VI) reduction is one of the mechanisms of U removal from solution, and that there is isotopic exchange between U(VI) and U(IV). The only known mechanism that induces U isotope fractionation at both the magnitude and direction observed in our experiments is the NFS and this can only occur in the presence of U(VI) and U(IV) at circumneutral pH. Since the reductant in the experiments is a solid and the experiments have a net transfer of aqueous U(VI) to solid U(IV) we infer that there must be isotopic exchange between the aqueous U(VI) and U(IV), possibly involving the mineral surfaces (*SI Appendix*, Figs. S3–S5). Thus, the isotopic fractionation can be manifested in the aqueous U(VI) pool via reversible weak sorption, likely to be the case in our experiments. An additional pathway for reduction is dissolution of FeS with U reduction by aqueous S^{-2}, but this mechanism is unlikely to be the primary pathway because the solubility of FeS is relatively low, and the kinetics of dissolution are slower than the observed U removal rates (43).

The magnitude of $^{238}U/^{235}U$ fractionation in the 2.0 mM Ca experiment is similar to the magnitude of $^{238}U/^{235}U$ fractionation in microbial U reduction experiments (6, 10, 39). Using the correlation between α and $U_{neutral}$, the predicted abiotic α at 100% neutral species is α = 1.00105 (±0.00005), which is statistically indistinguishable from the oxidation experiment value of 1.00110 (±0.00020) in acidic media (44). This result suggests that as the rate of U removal is slowed, the $^{238}U/^{235}U$ fractionation approaches the theoretical equilibrium values even in circumneutral pH solutions and with abiotic reductive precipitation. Our results establish U isotope ratios as a robust proxy for U(VI) reduction; however, based on this interpretation the observation of $^{238}U/^{235}U$ fractionation in natural systems cannot be viewed as a fingerprint of microbial U reduction as proposed by ref. 10.

Our experimental results are in apparent conflict with those of earlier studies of U isotope fractionation by abiotic reductants (3, 10, 18). The earlier studies found either no isotope fractionation or α < 1.0000. The primary difference between our experiments and earlier experiments is the rate at which U is removed from solution (Fig. 4). The timescale of the zerovalent zinc and iron experiments was 3 and 1 h, respectively, and while the FeS experiments of ref. 10 were up to 150 h, U removal from solution was nearly instantaneous via adsorption. Fig. 4 illustrates α as a function of the aqueous U(VI) half-life for our experimental results and for the prior studies (3, 10, 18, 44). We only include the FeS experiments from ref. 10 because U concentration and isotopic compositions can be described with a distillation model while the other solid-phase reductant experiments cannot. It is clear from Fig. 4 that the degree of U isotope fractionation is related to the overall rate of U removal from solution regardless of whether the initial removal step is primarily sorption or reduction. This observation suggests that the rate of U removal in earlier experiments (3, 10, 18) interfered with, and possibly inhibited, isotopic equilibrium during reduction [as hypothesized (3, 10, 18)]. To observe NFS U isotopic fractionation in the residual aqueous U(VI) the net removal rate from solution must be slow enough to allow for U isotopic equilibrium between U(VI) and U(IV). Rapid removal of aqueous U inhibits subsequent isotopic equilibrium during reduction between aqueous U and reduced U. The inhibition of isotopic equilibrium between sorbed U(VI) and sorbed U(IV) is evident because the experiments of ref. 10 had U sorbed to the mineral surface for three times longer than our longest experiment but still did not obtain the expected U isotope equilibrium between U(VI) and U(IV).

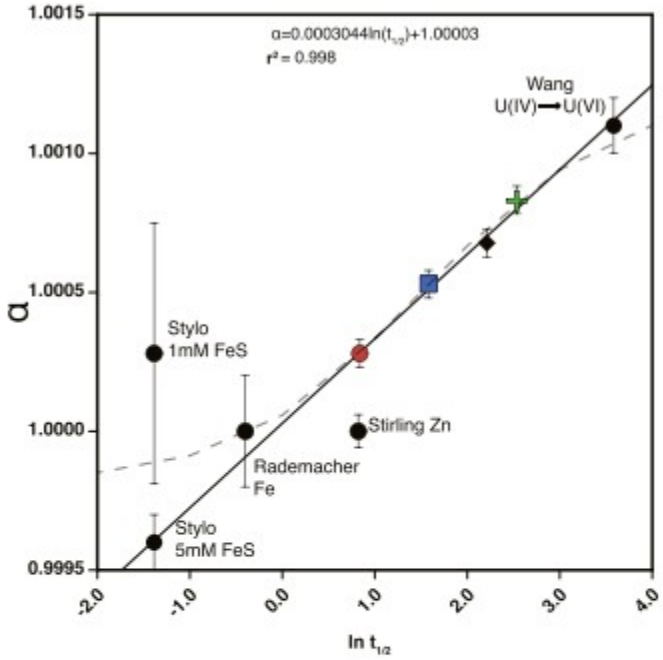

Fig. 4. Relationship between the half-life of aqueous U and the isotopic fractionation factor in our experiments and literature sources (3, 10, 18). Symbols for this study are the same as Fig. 1 and all literature experiments are labeled. The $t_{1/2}$ incorporates all mechanisms that remove U from solution. In the case of the ref. 10 experiments we inferred that $t_{1/2}$ must be ≤15 min based on the quantitative removal of aqueous U(VI) before their first reported analysis (30 min). The $t_{1/2}$ for refs. 3 and 18 were estimated from the reported concentration–time relationships. Curve fitting is to the present work, the 5-mM FeS reduction experiment by ref. 10 ($\alpha = 0.9996$), and the U(IV) oxidation experiment by ref. 44. A model curve (dashed gray line) reasonably fits the data and assumes that U reduction in the literature experiments is largely reflective of kinetic MDF effects and not NFS, whereas the experiments presented in this present work are intermediate between the two effects. See *SI Appendix* for a more detailed description of the model.

The U oxidation experiments of ref. 44 further support the conclusion that the half-life of the aqueous U reactant is important in controlling the magnitude of isotope fractionation during abiotic redox reactions. In aqueous U oxidation experiments of ref. 44 the half-life of oxidizing U(IV) is ~36 h and these experiments yield $\alpha = 1.0011$. Despite the different experimental approach the relationship between the U(IV) half-life and isotopic fractionation is consistent with the relationship determined from our experiments (Fig. 4). We can also hypothesize, based on the $t_{1/2}$–α relationship, that the necessary aqueous U half-life to achieve the predicted NFS fractionation of 1.3‰ at 300 K (16) is ~65 h.

The isotope fractionation that is expressed in the experiments on the left side of Fig. 4, especially the 5 mM FeS experiment, requires a fractionation mechanism that is different from the predicted NFS. The inferred α of less than 1.0000 and the fast removal rates suggest that kinetic mass-dependent fractionation may be important at faster U removal rates. One possible mechanism for kinetic MDF of U could be related to the desolvation and/or decarbonation of aqueous U species. Molecular dynamics simulations have

been used to demonstrate the importance of desolvation in the fractionation of isotopes for other cations in fluid mineral systems (e.g., ref. 45). Using the desolvation–fractionation relationship from ref. 45 (~0.5‰ for each percent mass difference between two isotopes) the desolvation-driven fractionation for U would be $\alpha = 0.99935$ compared with the maximum observed $\alpha = 0.9996 \pm 0.0001$ (Fig. 4 and ref. 10). In general, experimentally observed isotopic fractionation factors related to desolvation are partially attenuated compared with the simulated values, likely due to competing reaction steps (45).

Assuming that the observed $^{238}U/^{235}U$ fractionation at fast removal (Fig. 4) is primarily controlled by kinetic effects we can construct a model that interprets all of the experimental results as a balance between equilibrium isotope fractionation and kinetic isotope fractionation. The dashed gray curve in Fig. 4 is calculated using model parameters as described by DePaolo (46), namely, the relative forward and backward reaction rates and the limiting pure kinetic and pure equilibrium fractionation factors. Details of the modeling are provided in *SI Appendix*. The model predicts that at fast rates U isotope fractionation will be dominated by kinetic effects with an $\alpha < 1.0000$. In contrast, as the rate of U removal slows, the observed isotopic fractionation transitions to the equilibrium value, which is primarily a result of the NFS effect.

One possible way to confirm the competition between mass-dependent kinetic effects and the NFS effect with U isotope fractionation would be simultaneous high-precision measurements of both $^{238}U/^{234}U$ and $^{238}U/^{235}U$, as previously proposed by ref. 3. Since the NFS effect is disproportionately large for the ^{238}U–^{235}U isotope pair compared with the ^{238}U–^{234}U pair, the mass difference normalized fractionation of $^{238}U/^{235}U$ should increase relative to $^{238}U/^{234}U$ as the contribution of the NFS effect to the net isotope fractionation increases (15, 16).

Environmental and Geologic Implications.

The speciation-dependent model for U isotope fractionation has implications for interpreting $\delta^{238}U$ in the environment and the geologic record, as illustrated by the U isotopic record for the Black Sea. The Black Sea has been an important natural laboratory for studying element and isotopic distributions in anoxic water to make inferences about past periods of widespread anoxia in the global oceans (47). A recent study of the Black Sea water column found that the effective U isotopic fractionation is between ($\varepsilon^{238}U$) 0.63‰ and 0.84‰ depending on the applied fractionation model (48). In this study the deviation between the observed U isotope fractionation and the theoretical NFS value of ~1.3‰ is explained by diffusion-limited reduction in the sediments and back-diffusion of pore water U to the water column. Despite high concentrations of U(VI) reductants in the water column, any abiotic U removal in the water column was ruled out in previous studies. We calculated the U speciation using updated formation

constants, species (28), and prior published water column compositions for the Black Sea. The calculated fraction $U_{neutral}$ is 60% in modern Black Sea water, and the corresponding fractionation according to our model would be $\varepsilon^{238}U = 0.7‰$. The remarkably close agreement between field studies and our speciation-dependent fractionation model suggests that the aqueous speciation of U(VI) must be taken into account to determine the appropriate isotopic fractionation factor to interpret U isotope observations from the environment. In the case of the oceans, if the fraction of $U_{neutral}$ has changed over geologic time, as one might predict from changes in Ca/Mg, pCO_2, and pH, the isotopic fractionation factor during marine U reduction may have also changed and should be accounted for in models of paleoanoxia. Changes in speciation, however, are not likely to affect the U fractionation over short (<1 My) timescales since the residence time for Ca in the oceans is >1 My (49).

Several studies have used $\delta^{238}U$ to quantify the reduction of U(VI) in groundwater related to U mining and environmental contamination (5, 7, 50). In most studies the inferred U isotopic fractionation factor is significantly smaller than ($\varepsilon^{238}U$) 1.3‰, the theoretical NFS value. While the magnitude of U isotope fractionation is consistent with U reduction, quantifying the amount of reductive U precipitation compared with adsorption or other nonfractionating mechanisms is still a challenge. Applying our speciation–fractionation model to the groundwater at the Smith Ranch-Highlands U mine (7), we calculate an effective $\varepsilon^{238}U$ 0.7‰, similar to the value 0.78‰ inferred from variations in the $\delta^{238}U$ of site groundwater (7). The agreement between the observed and calculated $\varepsilon^{238}U$ suggests that at this particular site the removal of aqueous U(VI) from groundwater is primarily by reduction and that adsorption and hydrodynamic dispersion effects are small.

Materials and Methods

Experimental Methods.

All reagents and experiments were prepared inside a Coy Laboratory Products vinyl anaerobic chamber with an atmosphere of ~2.5% H_2–2.5% CO_2–95% N_2. Deionized water (18.2 MΩ) was degassed using industrial-grade N_2 and 2-μm-pore-sized diffusers for 1 h per liter of water. All remaining reagents were prepared from the degassed water.

FeS (Mackinawite) Synthesis.

FeS was synthesized by dissolving 18.37-g $FeCl_2$ powder and 11.73-g Na_2S powder in separate bottles containing 200 mL Milli-Q water (51). The solution was mixed by hand shaking several times over 3 d until the particles started to settle to the bottom of the container. The supernatant was poured off along with any suspended particles. The mixture was then resuspended in deionized (DI) water a total of three times to rinse away excess aqueous Fe and S. The final mixture was transferred to a serum bottle and sealed with butyl septa. Aliquots from this bottle were suspended in DI water in a syringe

and then pressed through a 0.2-μm syringe filter to remove particles smaller than 200 nm. The remaining particles from the filter were suspended in DI water and transferred to a clean serum bottle for storage. Well-mixed aliquots from this bottle were sampled with a 1-mL syringe and used for the uranium reduction experiments. Multiple 1-mL aliquots from this vial were sampled and weighed to determine the concentration of FeS in the stock solution. Multiple measurements yielded a mean concentration of 6 g/L. The purpose of selecting particles larger than 0.2 μm in diameter was to allow the complete separation of reactant and product at each sampling interval. FeS particles larger than 0.2 μm are likely aggregated smaller particles and likely have an effective surface area much higher than the nominal particle size suggests.

Uranium Reduction Experiments.

U reduction experiments were performed inside the same anaerobic chamber. All aqueous reagents were made with oxygen-free DI water and all containers were equilibrated in the anaerobic chamber for >48 h to remove adsorbed oxygen. Experimental solutions containing a 40 mL solution of $CaCl_2$–$NaHCO_3$–U were made in 50-mL centrifuge tubes. First $CaCl_2$ and $NaHCO_3$ solutions were diluted and mixed for 24 h to visually check for carbonate mineral precipitation. Next, ~80 μg of U [as $UO_2(CO_3)_2$] was added to the vials and mixed for 24 h to equilibrate the U–$CaCl_2$–$NaHCO_3$ solution. Mixed solutions were sampled before the addition of FeS and are labeled as time zero. FeS (3 mg) was added to the experiments and the vials were continuously mixed using an end-over-end rotator. One-milliliter samples were collected from the experiments on time intervals designed to sample across 0–90% of the U removal time. At each sampling interval the solution pH was measured. The pH of each experiment was 7.1 for the entire duration.

Uranium Purification.

Experimental solutions were spiked with IRMM 3636a ^{233}U–^{236}U double spike such that $^{238}U/^{236}U$ ~20. Solutions were dried down and subsequently dissolved in 3M HNO_3. Uranium purification was carried out using UTEVA resin in ~200-μL Teflon columns with HNO_3 and HCl as the eluants following published protocols (6).

Mass Spectrometry.

Purified uranium was analyzed on the Thermo Fisher NeptunePlus at Lawrence Berkeley National Laboratory. Solutions containing ~50 ng/g total U were introduced to the mass spectrometer using an ESI Apex fitted with an ACM module and a 100-μl/min nebulizer. The isotopic composition of U was quantified by static multicollection and referenced to the international standard Certified Reference Material CRM112a. Spike subtraction and U concentration calculations were completed using a single-step sample-spike deconvolution calculation (*SI Appendix*). The published isotopic compositions

are normalized to the time 0 sample from each experiment. Typical daily uncertainty on the $^{238}U/^{235}U$ standard is <0.1 and based on 6–12 measurements per session.

SEM.

A postexperiment filtrate of a single experiment was imaged with SEM and analyzed for elemental composition using energy-dispersive spectroscopy. The filtrate was not rinsed to avoid dissolving or oxidizing solid phases. As shown in *SI Appendix*, Figs. S3 and S4, plates of Fe-sulfide ranged up to ~100 µm in extent (compare S and Fe EDS maps). Also included in the filtrate are particles of NaCl and CaO, as indicated by the EDS elemental maps, likely formed with the drying of the filter from the experimental solution. Some FeS grains are associated with U, and usually the U is correlated with O, suggesting precipitation of uranium oxide. In the lower left of *SI Appendix*, Fig. S4is a grain of uranium oxide that is not associated with FeS, however in most instances U is directly associated with FeS. U concentrations on FeS grains were found to be up to ~20 wt % (*SI Appendix*, Fig. S5).

Acknowledgments

We benefited from the constructive comments of Francois Tissot on an earlier draft and from two anonymous reviewers. The project was initiated with support from the Laboratory Directed Research and Development program of Berkeley Laboratory, and completed with support from the Director, Office of Science, of the US Department of Energy under Contract DE-AC02-05CH11231.

References

1. Andersen MB, Stirling CH, Weyer S (2017) Uranium isotope fractionation. Rev Mineral Geochem 82:799–850.

2. Weyer S, Anbar AD, Gerdes A, Gordon GW (2008) Natural fractionation of 238 U/235 U. Geochim Cosmochim Acta 72:345–359.

3. Stirling CH, Andersen MB, Potter E-K, Halliday AN (2007) Low-temperature isotopic fractionation of uranium. Earth Planet Sci Lett 264:208–225.

4. Hiess J, Condon DJ, McLean N, Noble SR (2012) 238U/235U systematics in terrestrial uranium-bearing minerals. Science 335:1610–1614.

5. Murphy MJ, Stirling CH, Kaltenbach A (2014) Fractionation of 238U/235U by reduction during low temperature uranium mineralisation processes. Earth Planet Sci Lett 388: 306–317.

6. Basu A, Sanford RA, Johnson TM, Lundstrom CC, Löffler FE (2014) Uranium isotopic fractionation factors during U(VI) reduction by bacterial isolates. Geochim Cosmochim Acta 136:100–113.

7. Brown ST, et al. (2016) Isotopic evidence for reductive immobilization of uranium across a roll-front mineral deposit. Environ Sci Technol 50:6189–6198.

8. Tissot F, Dauphas N, Grove TL (2017) Distinct 238U/235U ratios and REE patterns in plutonic and volcanic angrites: Geochronologic implications and evidence for U isotope fractionation during magmatic processes. Geochim Cosmochim Acta 213: 593–617.

9. Tissot FLH, Dauphas N, Grossman L (2016) Origin of uranium isotope variations in early solar nebula condensates. Sci Adv 2:e1501400.

10. Stylo M, et al. (2015) Uranium isotopes fingerprint biotic reduction. Proc Natl Acad Sci USA 112:5619–5624.

11. Reinhard CT, Planavsky NJ, Olson SL, Lyons TW, Erwin DH (2016) Earth's oxygen cycle and the evolution of animal life. Proc Natl Acad Sci USA 113:8933–8938.

12. Christensen JN, Dresel PE, Conrad ME, Patton GW, DePaolo DJ (2010) Isotopic tracking of Hanford 300 area derived uranium in the Columbia River. Environ Sci Technol 44: 8855–8862.

13. Urey HC (1947) The thermodynamic properties of isotopic substances. J Chem Soc, 562–581.

14. Bigeleisen J, Mayer MG (1947) Calculation of equilibrium constants for isotopic exchange reactions. J Chem Phys 15:261–267.

15. Nomura M, Higuchi N, Fujii Y (1996) Mass dependence of uranium isotope effects in the U (IV)-U (VI) exchange reaction. J Am Chem Soc 118:9127–9130.

16. Bigeleisen J (1996) Nuclear size and shape effects in chemical reactions. Isotope chemistry of the heavy elements. Am Chem Soc 118:3676–3680.

17. Dujardin T, Lonchampt G (1990) Review of the French Chemex process. Available at https://inis.iaea.org/search/search.aspx?orig_q=RN:22063379. Accessed August 1, 2018.

18. Rademacher LK, et al. (2006) Experimentally determined uranium isotope fractionation during reduction of hexavalent U by bacteria and zero valent iron. Environ Sci Technol 40:6943–6948.

19. Maher K, Bargar JR, Brown GE, Jr (2013) Environmental speciation of actinides. Inorg Chem 52:3510–3532.

20. Liger E, Charlet L, Van Cappellen P (1999) Surface catalysis of uranium(VI) reduction by iron(II). Geochim Cosmochim Acta 63:2939–2955.

21. Stewart BD, Neiss J, Fendorf S (2007) Quantifying constraints imposed by calcium and iron on bacterial reduction of uranium(VI). J Environ Qual 36:363–372.

22. Ilton ES, et al. (2010) Influence of dynamical conditions on the reduction of U(VI) at the magnetite-solution interface. Environ Sci Technol 44:170–176.

23. Singer DM, et al. (2012) U(VI) sorption and reduction kinetics on the magnetite (111) surface. Environ Sci Technol 46:3821–3830.

24. Yuan K, Renock D, Ewing RC, Becker U (2015) Uranium reduction on magnetite: Probing for pentavalent uranium using electrochemical methods. Geochim Cosmochim Acta 156:194–206.

25. Fox PM, Davis JA, Zachara JM (2006) The effect of calcium on aqueous uranium (VI) speciation and adsorption to ferrihydrite and quartz. Geochim Cosmochim Acta 70: 1379–1387.

26. Brooks SC, et al. (2003) Inhibition of bacterial U(VI) reduction by calcium. Environ Sci Technol 37:1850–1858.

27. Rona E (1950) Exchange reactions of uranium ions in solution. J Am Chem Soc 72: 4339–4343.

28. Dong W, Brooks SC (2006) Determination of the formation constants of ternary complexes of uranyl and carbonate with alkaline earth metals (Mg2+, Ca2+, Sr2+, and Ba2+) using anion exchange method. Environ Sci Technol 40:4689–4695.

29. Endrizzi F, Rao L (2014) Chemical speciation of uranium(VI) in marine environments: Complexation of calcium and magnesium ions with [(UO2) (CO3)3](4-) and the effect on the extraction of uranium from seawater. Chemistry 20:14499–14506.

30. Behrends T, Van Cappellen P (2005) Competition between enzymatic and abiotic reduction of uranium (VI) under iron reducing conditions. Chem Geol 220:315–327.

31. Ulrich K-U, Veeramani H, Bernier-Latmani R, Giammar DE (2011) Speciationdependent kinetics of uranium(VI) bioreduction. Geomicrobiol J 28:396–409.

32. Lee J-Y, Yun J-I (2013) Formation of ternary CaUO2(CO3)3(2-) and Ca2UO2(CO3)3(aq) complexes under neutral to weakly alkaline conditions. Dalton Trans 42:9862–9869.

33. Bernhard G, et al. (2001) Uranyl (VI) carbonate complex formation: Validation of the Ca2UO2 (CO3) 3 (aq.) species. Radiochim Acta 89:511–518.

34. Chen X, Romaniello SJ, Herrmann AD, Wasylenki LE, Anbar AD (2016) Uranium isotope fractionation during coprecipitation with aragonite and calcite. Geochim Cosmochim Acta 188:189–207.

35. Chen X, Romaniello SJ, Anbar AD (2017) Uranium isotope fractionation induced by aqueous speciation: Implications for U isotopes in marine CaCO3 as a paleoredox proxy. Geochim Cosmochim Acta 215:162–172.

36. Han Y-S, Gallegos TJ, Demond AH, Hayes KF (2011) FeS-coated sand for removal of arsenic(III) under anaerobic conditions in permeable reactive barriers. Water Res 45: 593–604.

37. Wolthers M, Charlet L, van Der Linde PR, Rickard D, van Der Weijden CH (2005) Surface chemistry of disordered mackinawite (FeS). Geochim Cosmochim Acta 69: 3469–3481.

38. Scott KM, Lu X, Cavanaugh CM, Liu JS (2004) Optimal methods for estimating kinetic isotope effects from different forms of the Rayleigh distillation equation. Geochim Cosmochim Acta 68:433–442.

39. Stirling CH, Andersen MB, Warthmann R (2015) Isotope fractionation of 238 U and 235 U during biologically-mediated uranium reduction. Geochim Cosmochim Acta 163:200–218.

40. Hyun SP, Davis JA, Sun K, Hayes KF (2012) Uranium(VI) reduction by iron(II) monosulfide mackinawite. Environ Sci Technol 46:3369–3376.

41. Hua B, Deng B (2008) Reductive immobilization of uranium(VI) by amorphous iron sulfide. Environ Sci Technol 42:8703–8708.

42. Veeramani H, et al. (2013) Abiotic reductive immobilization of U(VI) by biogenic mackinawite. Environ Sci Technol 47:2361–2369.

43. Rickard D (2006) The solubility of FeS. Geochim Cosmochim Acta 70:5779–5789.

44. Wang X, Johnson TM, Lundstrom CC (2015) Isotope fractionation during oxidation of tetravalent uranium by dissolved oxygen. Geochim Cosmochim Acta 150:160–170.

45. Hofmann AE, Bourg IC, DePaolo DJ (2012) Ion desolvation as a mechanism for kinetic isotope fractionation in aqueous systems. Proc Natl Acad Sci USA 109:18689–18694.

46. DePaolo DJ (2011) Surface kinetic model for isotopic and trace element fractionation during precipitation of calcite from aqueous solutions. Geochim Cosmochim Acta 75: 1039–1056.

47. Arnold GL, Anbar AD, Barling J, Lyons TW (2004) Molybdenum isotope evidence for widespread anoxia in mid-Proterozoic oceans. Science 304:87–90.

48. Rolison JM, Stirling CH, Middag R, Rijkenberg MJA (2017) Uranium stable isotope fractionation in the Black Sea: Modern calibration of the 238U/235U paleo-redox proxy. Geochim Cosmochim Acta 203:69–88.

49. Broecker WS, Peng TH (1982) Tracers in the Sea (Eldigio Press, New York).

50. Basu A, et al. (2015) Isotopic and geochemical tracers for U (VI) reduction and U mobility at an in situ recovery U mine. Environ Sci Technol 49:5939–5947.

51. Butler EC, Hayes KF (1998) Effects of solution composition and pH on the reductive dechlorination of hexachloroethane by iron sulfide. Environ Sci Technol 32: 1276–1284.